

Exploring the Potential of Oblique UAV Imagery for Wildfire Risk Assessment: Comparative Analysis between Nadir and Oblique Images

Michal Aibin*, Yue Chang†, Chen Chen†, Manping Zhao†

Ruidi Huang†, Siqi Chen†, Cuiting Huang†, Sujit Nashik†, Victor Wu†

*Department of Computing, British Columbia Institute of Technology, maibin@bcit.ca

†Khoury College of Computer Sciences, Northeastern University, vancouver@northeastern.edu

Abstract—Wildfire is a serious threat to forest ecosystems, particularly in forested environments with complex vertical structures. This study explores the potential of oblique UAV imagery to enhance wildfire risk prediction by comparing their performance against nadir imagery. In this study, we apply state-of-the-art segmentation algorithms, analyzing their precision in identifying predefined flammable objects such as dead trees, debris and beetle-damaged trees in nadir and oblique imagery. The results show that the oblique images provide an angled perspective with more features, thereby improving the accuracy of the flammability risk assessments. This research underscores the importance of using oblique imagery for wildfire assessment, paving the way for efficient wildfire management strategies.

Index Terms—UAV, Computer Vision, Wildfire Prediction

I. INTRODUCTION

Wildfires have significant impacts on property, cultural values, ecological values, infrastructure, local economies, and people's health and well-being. In British Columbia, Canada, the numbers are alarming: From 2011 to 2020, an average of 1,483 wildfires were ignited each year. The financial and environmental toll is staggering, with total damages estimated at \$4.83 billion Canadian dollars over the decade [1]. In the past, wildfire prediction relied on weather data and historical occurrences, which often lacked the precision and timeliness needed for effective intervention. Recent progress in object detection, using ML and DL techniques integrated with UAV-based data, has demonstrated potential in wildfire prediction.

Most research using unmanned aerial vehicles (UAVs) uses nadir imagery primarily [2]–[6]. Nadir imagery, which is captured from directly overhead, provides a bird's eye view of the terrain but may not capture the depth and detailed perspective necessary for comprehensive analysis. In contrast, oblique imagery is taken at an angle and provides better perspectives by depicting both vertical and horizontal structures.

However, existing work on oblique imagery focuses mainly on built-up environments and structural damage surveys, leaving natural landscapes under-investigated for wildfire analysis [7]–[10]. Much of this research addresses building collapse detection, urban monitoring, or other infrastructure concerns, rather than wildfire scenarios. Furthermore, despite advances in the prediction and detection of wildfires using various ML and DL techniques [11], there is no comparative analysis evaluating the effectiveness of nadir and oblique imagery.



Fig. 1: Identifying points of interest for flammability detection using UAV imagery.

In the context of wildfire prediction, oblique views have the potential to identify common flammable objects on the terrain, such as dead trees, debris and Japanese beetle-damaged trees, that might not be visible in a bird's-eye view. Consequently, there is a clear research gap in comparing the oblique and nadir perspectives to identify flammable objects more effectively for wildfire modeling [12]. Conducting a comparative study could clarify whether oblique images provide more details, making them a preferable input for wildfire prediction models.

II. LITERATURE REVIEW

Recent advances in ML and DL have significantly improved wildfire prediction accuracy and efficiency by addressing challenges in prediction and segmentation. CNNs integrated with traditional ML techniques, such as SE-ResNet with SVMs, improve the precision of smoke prediction by distinguishing patterns from atmospheric anomalies [13]. Optimized YOLO models (e.g., YOLO v5, YOLO v7x, YOLO v8s) improve early smoke prediction based on UAV, reduce false alarms, and perform well in diverse terrains and small fire areas [14], [15]. Hybrid approaches, such as YOLO v5 with U-Net, improve the segmentation accuracy for small fire objects [16]. Vision transformers, such as TransUNet and TransFire, combined with EfficientNet-B5 and DenseNet-201, achieve high precision in

wildfire classification and segmentation, capturing fine details from complex environments [17], [18].

UAV imagery supports forest monitoring and wildfire fuel detection by providing real-time information and improving risk evaluation. Systems such as those of Bailon-Ruiz et al. [19] use UAVs to monitor the spread of wildfires and plan the trajectory, while LDS-YOLO detects dead trees in shelter forests [20]. Enhanced YOLOv8 models effectively classify tree species using multisource data [21], and integrated frameworks visualize forest fire risks with UAV imagery and color mapping [12]. Oblique aerial images, discussed by Verykokou and Ioannidis [22], complement nadir imagery by capturing structural details, with applications ranging from individual tree detection to disaster damage assessment using advanced DL models [7], [10], [23].

Water sources play a critical role in the management of wildfires by influencing nearby soil moisture levels, which affect the spread of the fire [24], [25]. Index-based methods, such as NDWI [26] and MNDWI [27], highlight water bodies but face challenges in complex environments. Deep learning methods, such as MC-WBDN [28], SegNet [29], and U-Net [30], achieve high accuracy and adaptability, with advanced architectures such as SegFormer-U-Net further enhancing segmentation in challenging scenarios [31].

Despite significant advances in wildfire prediction, there remains a research gap in the application of these models to identify oblique imagery. Since oblique images capture a broader perspective both horizontally and vertically, they can offer more information than conventional nadir images. Bearing this in mind, our research seeks to build upon an existing understanding of predefined flammable objects and investigate the possibility of enhancing the detection of such objects using oblique images, ultimately improving the input for wildfire prediction models that rely on flammable objects.

III. PROBLEM STATEMENT

Accurate prediction of wildfires is critical for timely intervention and risk mitigation. UAV imagery has become an essential tool for the assessment of wildfire risk, providing high-resolution data to detect flammable objects. However, most existing models rely on nadir imagery (top-down view), which lacks vertical structural details crucial for comprehensive fire risk modeling. Oblique imagery, captured at an angle, has the potential to improve segmentation accuracy by incorporating additional spatial information. A comparison of these two types of images can be seen in Figure 2.

To better understand how nadir and oblique imagery contribute to wildfire risk assessment, we present a workflow pipeline outlining the key stages from image acquisition to wildfire prediction seen in Figure 3.

The study evaluates whether integrating oblique imagery enhances wildfire risk assessment of two key elements:

- **Points of Interest (POIs)** – Flammable objects, including dead trees, debris and beetle-fire trees.
- **Water sources** – Natural firebreaks that help mitigate wildfire spread.



(a) Nadir image



(b) Oblique image

Fig. 2: A comparison of (a) nadir image and (b) oblique image.

Using advanced deep learning segmentation models (*Mask2Former* and *Mask R-CNN*), this research compares nadir and oblique image performance to quantify segmentation accuracy for nadir vs. oblique imagery, assess whether oblique images capture finer structural details, and evaluate the impact of improved segmentation on wildfire risk estimation.

There are three POIs (shown in Figure 4) that this paper seeks to detect because they are key flammable objects:

- **Dead trees** – Dry, standing trees with high fire risk. They are identified by their lack of foliage, withered branches, and decaying trunks.
- **Debris** – Fallen branches and vegetation that contribute to fuel load. Consists of fallen branches and vegetation scattered on the ground, differing primarily in their orientation.
- **Beetle-impacted trees** – Vegetation weakened by infestation, increasing fire susceptibility. They show golden, red, or orange hues due to Japanese beetle infestation, making them visually distinct but challenging to classify.

Meanwhile, water sources (as shown in Figure 5) such as streams and ponds appear as smooth, reflective surfaces and are essential in wildfire risk reduction.

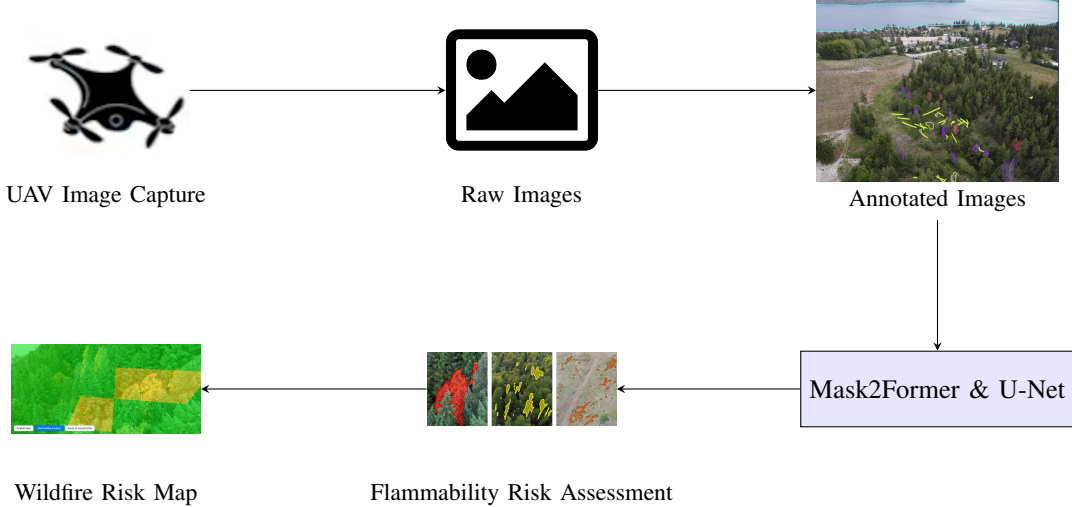


Fig. 3: Workflow pipeline for UAV-based wildfire risk assessment, integrating raw and annotated images into segmentation and risk evaluation.

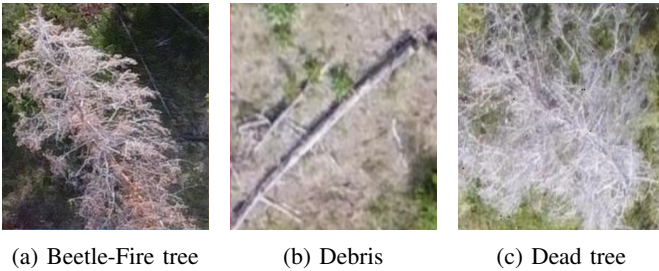


Fig. 4: Examples of flammable objects: (a) beetle-fire tree, (b) debris, (c) dead tree.



Fig. 5: Example of a water source, outlined in cyan.

IV. ALGORITHMS

This section describes how we used two deep learning models, Mask2Former and U-Net, to detect flammable objects in forest imagery and to segment water bodies. Both tasks benefit from similar strategies, including the use of high-resolution UAV imagery, class weighting to address imbalances, and data tiling for efficient processing. However, each model and task have unique considerations that we discuss below.

A. Mask2Former and U-Net Overview

We employed Mask2Former, a transformer-based segmentation framework, to handle complex shapes within cluttered backgrounds. Using masked attention to highlight regions likely to contain target objects, we found it particularly effective in dense forest settings. We fine-tuned Mask2Former on tiled UAV images for both flammable object detection and water segmentation, preserving high-resolution detail without relying on extensive data augmentations, using architecture shown in Figure 6.

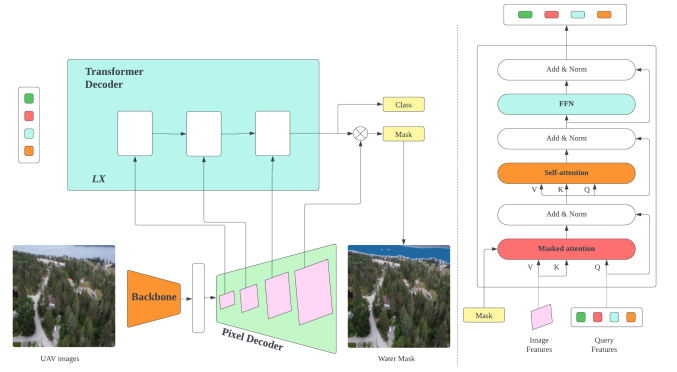


Fig. 6: The architecture of our Mask2former model.

We also used U-Net, which has an encoder-decoder structure with skip connections that preserve spatial information while reducing resolution. This architecture is well suited for precise boundary detection. We configured U-Net to address class imbalance by assigning higher weights to less common categories, such as debris or water regions, helping the model to better focus on underrepresented classes in large forest scenes. We used U-Net with a pre-trained EfficientNet-B3 backbone in the encoder and transposed convolutions plus skip

connections in the decoder to refine boundaries, as illustrated in Figure 7.

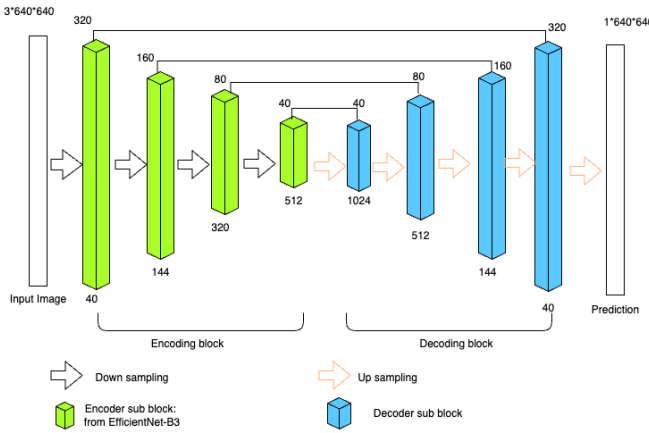


Fig. 7: The architecture of our U-Net model

B. POIs and Water Source Segmentation

POIs include flammable objects such as dead trees, debris and beetle-fire trees. We trained Mask2Former and U-Net in high-resolution UAV imagery labeled for these specific categories. Mask2Former relies on masked attention to locate irregular targets such as debris in crowded forests. A class-specific weighted loss function was important for dealing with a lower representation of categories such as beetle-fire trees. U-Net employs its default encoder-decoder design, and skip connections preserve shape details of dead trees and debris. We applied a weighted cross-entropy loss to further address the imbalance among POIs classes.

Water bodies serve as natural barriers in wildfire scenarios, but segmenting them still requires accounting for the varying shapes of the shorelines. We applied weighted loss to improve the recognition of smaller water regions.

C. Performance Metrics

We assess the model's segmentation performance on *dead trees*, *debris*, *beetle-fired trees*, and the *null class* using common six key metrics: *Intersection over Union (IoU)*, *accuracy*, *Dice coefficient*, *F-score*, *precision*, and *recall* [32]:

Intersection over Union (IoU) measures the overlap between the predicted (M_p) and the ground truth mask (M_{gt}):

$$IoU = \frac{|M_p \cap M_{gt}|}{|M_p \cup M_{gt}|}. \quad (1)$$

Higher IoU values indicate better alignment between the predictions and the ground truth.

Precision quantifies the proportion of correctly predicted positive pixels out of all pixels predicted as positive:

$$Precision = \frac{TP}{TP + FP}. \quad (2)$$

Recall measures the proportion of correctly predicted positive pixels out of all actual positive pixels:

$$Recall = \frac{TP}{TP + FN}. \quad (3)$$

Dice Coefficient and **F-score** provide a balance between precision and recall:

$$Dice = \frac{2 \cdot TP}{2 \cdot TP + FP + FN}, \quad (4)$$

$$Fscore = 2 \cdot \frac{Precision \cdot Recall}{Precision + Recall}. \quad (5)$$

Accuracy represents the overall proportion of correctly classified pixels:

$$Accuracy = \frac{TP + TN}{TP + TN + FP + FN}. \quad (6)$$

Together, these metrics provide a comprehensive evaluation of the model's segmentation capabilities, ensuring robust performance analysis across all target classes.

V. SIMULATION SETUP

We used a dataset of 462 UAV-captured images with a median resolution of $4,000 \times 3,000$ pixels. It supports two main tasks: POIs detection and water segmentation. The POIs dataset has 3,822 annotations across beetle-fired trees, debris and dead trees, averaging 8.3 annotations per image. The other 45 images do not have target classes. Debris lies on the ground, dead trees remain standing without foliage, and beetle-fired trees show golden or red hues due to insect damage. To refine training, each original image was split into a 4×4 grid, producing 18,730 smaller tiles.

For water segmentation, there are 405 water annotations. Water sources often appear reflective and bounded by vegetation. When water segmentation models are trained, flammable objects are treated as null, with the focus on water. This arrangement ensures robust detection of flammable materials while also isolating water bodies, which can serve as natural barriers to fire spread.

VI. RESULTS

In this section, we present the numerical findings of our experiments and offer a detailed discussion of each table. We also provide a subsection on the visualization of segmentation results, illustrating how Mask2Former and U-Net perform in detecting POIs and segmenting water bodies.

A. Numerical Outcomes and Discussion

Table I details the Mask2Former performance in detecting various POI. The model clearly distinguishes non-flammable regions, as reflected by the high IoU (96.91%) and accuracy (98.34%) for the *null* class. This indicates that Mask2Former excels at filtering out irrelevant background pixels, providing a strong baseline for wildfire risk assessments.

TABLE I: Performance Metrics for POIs Detection of Mask2Former (Oblique Images)

Class	IoU (%)	Acc (%)	Dice (%)	Fscore (%)	Precision (%)	Recall (%)
null	96.91	98.34	98.43	98.43	98.52	98.34
beetle-fire	46.21	85.62	63.21	63.21	50.10	85.62
dead-tree	20.44	23.49	33.94	33.94	61.17	23.49
debris	20.24	33.07	33.67	33.67	34.28	33.07

Looking at flammable categories, beetle-fire shows a moderate IoU (46.21%) but achieves a much higher recall of 85.62%. This suggests that the model rarely misses beetle-fire pixels, capturing most of these objects in the image. However, its precision is lower (50.10%), implying that, while the model is sensitive to beetle-fire trees, it occasionally misclassifies other elements in the scene as beetle-fire. For dead trees, the IoU is 20.44%, but the model reaches a relatively good precision of 61.17%. In practical terms, whenever Mask2Former predicts a dead-tree pixel, it is correct more than half the time. The challenge remains to increase the recall (23.49%), as many dead tree pixels are still missing. This may be due in part to the way that dead trees vary in shape, color, and position relative to living trees. Finally, the debris shows somewhat balanced precision and recall values in the low to mid range 30%, leading to an IoU of 20.24%. Debris in forested areas can appear in scattered clusters or be partially covered by foliage, which complicates consistent detection.

Table II demonstrates the performance of the U-Net model to detect POIs in oblique UAV images. Compared to Mask2Former, U-Net consistently shows lower segmentation performance across all classes. For the null class, U-Net achieves an IoU of 60.15%, which is substantially lower than Mask2Former’s 96.91%. Similarly, for the detection of flammable objects, U-Net records an IoU of 13.22% for trees that have burned beetle, 15.24% for dead trees and 12.22% for debris, all of which are significantly lower than the corresponding IoU values obtained by Mask2Former.

TABLE II: Performance Metrics for POIs Detection using U-Net (Oblique images)

Class	IoU (%)	Acc (%)	Dice (%)	Fscore (%)	Precision (%)	Recall (%)
null	60.15	61.05	75.19	75.19	99.02	60.56
beetle-fire	13.22	24.50	23.36	23.36	24.12	22.62
dead-tree	15.24	17.50	26.45	26.45	23.55	30.16
debris	12.22	20.00	21.78	21.78	77.13	12.67

Furthermore, U-Net’s Dice and F score metrics, which are 75.19% for the null class and range between 21.78% and 26.45% for the flammable classes, indicate a weaker balance between precision and recall compared to Mask2Former. Although U-Net achieves high precision for the null class (99.02%), its precision for the flammable classes remains low. These discrepancies suggest that Mask2Former is better suited for wildfire risk assessment, as it provides a more balanced and reliable segmentation of critical flammable objects, particularly debris, a key fire hazard often underdetected by U-Net.

Tables III and IV compare Mask2Former’s segmentation performance for oblique versus nadir imaging. We see consistent gains in all metrics when using oblique viewpoints. For example, debris segmentation increases its IoU from 15.21% at the nadir to 20.24% at the oblique, while the dead tree also shows noticeable growth (from 18.21% to 20.44% IoU). Even beetle-fire, which achieves moderate accuracy and recall in nadir views, benefits from oblique angles, improving its IoU from 41.26% to 46.21%.

These improvements extend beyond IoU. For debris, precision jumps from 25.71% to 34.28%, and recall rises from 24.80% to 33.07%. Similarly, beetle-fire sees higher precision (44.59% to 50.10%) and recall (76.31% to 85.62%), which together boost its F-score by nearly seven percentage points. These positive changes indicate that angled UAV imagery helps capture additional surface and shape details, allowing the model to better distinguish objects from their backgrounds.

Oblique viewpoints seem to reveal more visible edges and height cues, which prove especially helpful for irregular or partially obscured targets like fallen debris and dead trees. Although nadir images are standard for many mapping applications, these results strongly suggest that including oblique imagery can substantially enhance segmentation outcomes in wildfire-related analyses.

TABLE III: Performance Metrics for POIs Detection (IoU, Dice, and Accuracy: Oblique vs. Nadir)

Class	IoU (%)		Dice (%)		Acc (%)	
	Oblique	Nadir	Oblique	Nadir	Oblique	Nadir
null	96.91	85.22	98.43	88.59	98.34	83.59
beetle-fire	46.21	41.26	63.21	58.39	85.62	76.31
dead-tree	20.44	18.21	33.94	30.83	23.49	20.78
debris	20.24	15.21	33.67	26.43	33.07	24.80

TABLE IV: Performance Metrics for POIs (Precision, Recall, and Fscore: Oblique vs. Nadir)

Class	Precision (%)		Recall (%)		Fscore (%)	
	Oblique	Nadir	Oblique	Nadir	Oblique	Nadir
null	98.52	85.58	98.34	84.77	98.43	83.59
beetle-fire	50.10	44.59	85.62	76.31	63.21	56.43
dead-tree	61.17	54.34	23.49	20.91	33.94	30.21
debris	34.28	25.71	33.07	24.80	33.67	25.25

Table V summarizes these improvements for each metric. Debris experiences the largest leap, with more than 30% gains in IoU and accuracy. We think this is because debris pieces often lie on the forest floor or near tree trunks, which become more discernible from oblique angles. Smaller improvements for beetle-fire and dead-tree may be due to shared color and texture with surrounding vegetation, which can still be partially obscured from any angle.

Table VI shows the metrics for water segmentation. U-Net with an EfficientNet-B3 backbone achieves an IoU of 84.47% and a Dice of 91.58%, indicating it reliably isolates water from forested regions. Mask2Former attains a higher IoU (92.81%) and Dice (96.27%) but records a slightly lower accuracy (97.58%). We think this difference occurs because Mask2Former focuses on accurately outlining water edges, which can reduce total accuracy if a few small regions are misclassified. However, both models perform strongly, and identifying water bodies is crucial for planning wildfires.

We did not include a comparison of oblique versus nadir images for water segmentation due to space limitations, but the outcomes follow a similar trend: oblique viewpoints help capture boundary details, improving segmentation metrics.

TABLE V: Performance Metrics Improvement from Nadir to Oblique (Percentage)

Class	IoU Improvement (%)	Dice Improvement (%)	Acc Improvement (%)	Precision Improvement (%)	Recall Improvement (%)	Fscore Improvement (%)
null	13.71	11.11	17.65	15.11	16.00	17.76
beetle-fire	12.00	8.25	12.20	12.34	12.20	12.03
dead-tree	12.23	10.09	13.05	12.58	12.34	12.33
debris	33.08	27.40	33.38	33.33	33.38	33.33

TABLE VI: Performance Metrics for Water Segmentation

Model	IoU (%)	Acc (%)	Dice (%)	Fscore (%)	Precision (%)	Recall (%)
Unet with Efficientnet b3	84.47	99.16	91.58	91.58	93.86	93.75
Mask2Former	92.81	97.58	96.27	96.27	91.67	92.88

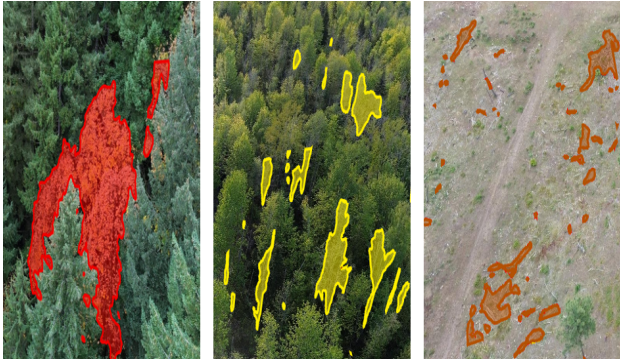


Fig. 8: POI Color Coding

VII. VISUALIZATION FOR WILDFIRE RISK ASSESSMENT

Our unified visualization approach for the assessment of wildfire risk combines detailed POI identification with a complete visualization of the risk of the flammability gradient, using spherical UAV images. The methodologies applied are discussed in detail in the subsequent subsections.

A. Image Tiling

The process begins with the transformation of spherical UAV images into a series of 512x512 pixels tiles at various zoom levels. Specifically, we use zoom level 3, which optimally balances the level of detail and the area covered per tile, ensuring that each tile retains the necessary detail for accurate feature analysis and risk assessment.

B. Point of Interest Visualization

Each tile undergoes an analysis using a deep learning model to predict POI. The detected POIs are then marked distinctly using a color-coded scheme, beetle-fire trees are highlighted in red, debris in brown, and dead trees in yellow, as shown in Figure 8. Following the analysis, the tiles are stitched together to reconstruct the spherical image. For visualization in the Marzipano viewer, the coordinates of these POIs are converted into pitch and yaw values, which facilitate accurate representation in a three-dimensional space (see Figure 9).

C. Flammability Percentage

To enhance fire risk management and prevention strategies, we developed a sophisticated flammability percentage system. The flammability percentage is measured by assessing the ratio of potential ignition sources (POIs) to areas populated by alive



Fig. 9: POI Visualization

trees and regions with water content. On this scale where a percentage of 0 signifies no fire risk, and a percentage of 100 represents absolute certainty of a forest fire. This system employs an overlay technique on panoramic UAV imagery to visually represent the flammability risks across various landscape regions. It integrates a color-coded gradient overlay that couples quantitative risk percentages with visual cues as referenced in Table VII.

TABLE VII: Flammability Percentage Color Indicators

Range(%)	Risk Level	Color
0-5	Low	Green
6-25	Moderate	Yellow
26-60	High	Orange
61-80	Very High	Red
81-100	Extreme	Dark Red

D. Flammability Gradient Visualization

In the process of generating the flammability gradient, the initial step involves the identification of POIs. Following this, we calculate the percentage of flammability for each identified POI. Subsequently, each tile is color coded based on its assessed flammability risk, enhancing the ease of visual interpretation. Finally, these color-coded tiles are stitched together to form a spherical image. For visualization, the image is overlaid onto the panorama in the Marzipano viewer, as illustrated in Figure 10.

VIII. CONCLUSION AND FUTURE WORK

This study shows that oblique UAV imagery can greatly improve wildfire prediction by offering more nuanced views of flammable objects. Compared to nadir imagery, oblique angles consistently yield higher detection rates for beetle-fire trees, dead trees, and debris, benefiting from the additional height and side details visible in angled shots. Advanced



Fig. 10: Flammability Gradient Visualization

deep learning models (Mask2Former and U-Net) confirm these gains through improved Intersection over Union (IoU) and Dice coefficients in identifying critical wildfire-fuel elements.

Although the results clearly demonstrate the benefits of oblique perspectives, challenges remain. Increased computational requirements, lighting variations, and the need for a larger and more diverse dataset point to directions for future work. Integrating oblique and nadir viewpoints in a single hybrid model, together with time-series data, could extend the precision and generalizability of these findings. In general, this work underscores the importance of using oblique imagery in UAV-based wildfire risk assessments, paving the way for more robust and proactive fire management strategies.

ACKNOWLEDGMENT

This work was supported by the Mitacs grant IT39827 and the statutory funds of the BC Institute of Technology. We also acknowledge the help from our industry partner, Spexi.

REFERENCES

- [1] G. of British Columbia. (2022) Wildfire averages. Accessed: 3-Feb-2025. [Online]. Available: <https://www2.gov.bc.ca/gov/content/safety/wildfire-status/about-bcws/wildfire-statistics/wildfire-averages>
- [2] S. Puliti *et al.*, “Automatic detection of snow breakage at single tree level using yolov5 applied to uav imagery,” *International Journal of Applied Earth Observation and Geoinformation*, vol. 112, p. 102946, 2022.
- [3] D. Rashkovetsky *et al.*, “Wildfire detection from multisensor satellite imagery using deep semantic segmentation,” *IEEE Journal of Selected Topics in Applied Earth Observations and Remote Sensing*, vol. 14, pp. 7001–7016, 2021.
- [4] Z. Yang *et al.*, “Next-Gen Remote Airport Maintenance: UAV-Guided Inspection and Maintenance Using Computer Vision,” *Drones*, vol. 8, no. 6, p. 225, 2024.
- [5] R. Sharma *et al.*, “Aerial footage analysis using computer vision for efficient detection of points of interest near railway tracks,” *Aerospace*, vol. 9, no. 7, 2022. [Online]. Available: <https://www.mdpi.com/2226-4310/9/7/370>
- [6] ———, “Real-time search and rescue using remotely piloted aircraft system with frame dropping,” in *2023 International Conference on Computing, Networking and Communications (ICNC)*, 2023, pp. 83–88.
- [7] Y. Lin *et al.*, “Use of uav oblique imaging for the detection of individual trees in residential environments,” *Urban forestry & urban greening*, vol. 14, no. 2, pp. 404–412, 2015.
- [8] A. Vetrivel *et al.*, “Disaster damage detection through synergistic use of deep learning and 3d point cloud features derived from very high resolution oblique aerial images, and multiple-kernel-learning,” *ISPRS journal of photogrammetry and remote sensing*, vol. 140, pp. 45–59, 2018.
- [9] S. Verykokou *et al.*, “Oblique aerial images: a review focusing on georeferencing procedures,” *International journal of remote sensing*, vol. 39, no. 11, pp. 3452–3496, 2018.
- [10] H. Hart, “Extracting fire behaviour data from georeferenced oblique aerial wildfire photographs,” Ph.D. dissertation, 2022.
- [11] L. Ramos *et al.*, “Computer vision for wildfire detection: a critical brief review,” *Multimedia Tools and Applications*, pp. 1–44, 2024.
- [12] M. Aibin *et al.*, “Advancing forest fire risk evaluation: An integrated framework for visualizing area-specific forest fire risks using uav imagery, object detection and color mapping techniques,” *Drones*, vol. 8, no. 2, p. 39, 2024.
- [13] X. Wang *et al.*, “Improving computer vision-based wildfire smoke detection by combining se-resnet with svm,” *Processes*, vol. 12, no. 4, 2024. [Online]. Available: <https://www.mdpi.com/2227-9717/12/4/747>
- [14] M. Mukhiddinov *et al.*, “A wildfire smoke detection system using unmanned aerial vehicle images based on the optimized yolov5,” *Sensors*, vol. 22, no. 23, p. 9384, 2022.
- [15] L. A. O. Gonçalves *et al.*, “Yolo-based models for smoke and wildfire detection in ground and aerial images,” *Fire*, vol. 7, no. 4, 2024. [Online]. Available: <https://www.mdpi.com/2571-6255/7/4/140>
- [16] W. S. Mseddi *et al.*, “Fire detection and segmentation using yolov5 and u-net,” in *2021 29th European Signal Processing Conference (EUSIPCO)*. IEEE, 2021, pp. 741–745.
- [17] R. Ghali *et al.*, “Wildfire segmentation using deep vision transformers,” *Remote Sensing*, vol. 13, no. 17, 2021. [Online]. Available: <https://www.mdpi.com/2072-4429/13/17/3527>
- [18] ———, “Deep learning and transformer approaches for uav-based wildfire detection and segmentation,” *Sensors*, vol. 22, no. 5, p. 1977, 2022.
- [19] R. Bailon-Ruiz *et al.*, “Real-time wildfire monitoring with a fleet of uavs,” *Robotics and Autonomous Systems*, vol. 152, p. 104071, 2022.
- [20] X. Wang *et al.*, “Lds-yolo: A lightweight small object detection method for dead trees from shelter forest,” *Computers and Electronics in Agriculture*, vol. 198, p. 107035, 2022.
- [21] H. Zhong *et al.*, “Individual tree species identification for complex coniferous and broad-leaved mixed forests based on deep learning combined with uav lidar data and rgb images,” *Forests*, vol. 15, no. 2, p. 293, 2024.
- [22] S. Verykokou *et al.*, “Oblique aerial images: Geometric principles, relationships and definitions,” *Encyclopedia*, vol. 4, no. 1, pp. 234–255, 2024.
- [23] X. Deng *et al.*, “Detection and location of dead trees with pine wilt disease based on deep learning and uav remote sensing,” *AgriEngineering*, vol. 2, no. 2, pp. 294–307, 2020.
- [24] L. Bruckler *et al.*, “Near surface soil moisture estimation from microwave measurements,” *Remote Sensing of Environment*, vol. 26, pp. 101–121, 1988.
- [25] A. Crave *et al.*, “The influence of topography on time and space distribution of soil surface water content,” *Hydrological Processes*, vol. 11, pp. 203–210, 1997.
- [26] S. K. McFEETERS, “The use of the normalized difference water index (ndwi) in the delineation of open water features,” *International Journal of Remote Sensing*, vol. 17, no. 7, pp. 1425–1432, 1996.
- [27] H. Xu, “Modification of normalised difference water index (ndwi) to enhance open water features in remotely sensed imagery,” *International Journal of Remote Sensing*, vol. 27, no. 14, pp. 3025–3033, 2006.
- [28] K. Yuan *et al.*, “Deep-learning-based multispectral satellite image segmentation for water body detection,” *IEEE Journal of Selected Topics in Applied Earth Observations and Remote Sensing*, vol. 14, pp. 7422–7434, 2021.
- [29] T. S. Akiyama *et al.*, “Deep learning applied to water segmentation,” *The International Archives of the Photogrammetry, Remote Sensing and Spatial Information Sciences*, vol. XLIII-B2-2020, pp. 1189–1193, 2020. [Online]. Available: <https://isprs-archives.copernicus.org/articles/XLIII-B2-2020/1189/2020/>
- [30] P. Likhitosh *et al.*, “U-net based semantic segmentation of still water bodies using aerial images,” in *2024 International Conference on Computational Intelligence for Green and Sustainable Technologies (ICCIGST)*, 2024, pp. 1–6.
- [31] Z. Xie *et al.*, “Application of deep learning techniques in water level measurement: Combining improved segformer-unet model with virtual water gauge,” *Applied Sciences*, vol. 13, no. 9, p. 5614, 2023. [Online]. Available: <https://www.mdpi.com/2076-3417/13/9/5614>
- [32] M. Karimibiki *et al.*, “Drones’ face off: Authentication by machine learning in autonomous iot systems,” in *2019 IEEE 10th Annual Ubiquitous Computing, Electronics Mobile Communication Conference (UEMCON)*, 2019, pp. 0329–0333.